 https://doi.org/10.3311/PPee.22592

Periodica Polytechnica Electrical Engineering and Computer Science, 68(2), pp.124–134, 2024

Numerical Study of the Influence of Using Semicircular Corrugated Collecting Plate and Inverted Semicircular Corrugated on the Electrostatic Precipitator

Moath Bani Fayyad[1*], Tamás Iváncsy[1]

[1] Department of Electric Power Engineering, Faculty of Electrical Engineering and Informatics, Budapest University of Technology and Economics, Műegyetem rkp. 3., H-1111 Budapest, Hungary
[*] Corresponding author, e-mail: mbanifayyad@edu.bme.hu

Received: 15 May 2023, Accepted: 07 November 2023, Published online: 27 February 2024

Abstract

Electrostatic precipitators (ESPs) play a crucial role in removing harmful particles in various industries. Ongoing studies continuously strive to improve their performance and efficiency, leveraging the inherent advantages of ESPs. Researchers are exploring various types of collecting and discharge electrodes to achieve this. This study specifically focuses on comparing two types of collecting electrodes, Semicircular Corrugated Plates (SCPs) and inverted Semicircular Corrugated Plates (InvSCPs), against Flat Plates (FPs) as a reference case. Three distinct forms of ESPs were simulated, and the SCP and InvSCP designs were evaluated against the FPs, specifically assessing the impact of modifying the collecting electrode design on key electrostatic precipitator characteristics, such as electrical field distribution, space charge density distribution, particle trajectories, and particle collection efficiency. Notably, the study found that using SCP resulted in the highest particle collection efficiency compared to InvSCP and FP for the same range of particles.

Keywords

corona discharge, collecting electrode, electrostatic precipitators

1 Introduction

Particulate emissions are one of the most urgent problems with air pollution, which has become a serious concern for everyone. In a variety of industrial fields, electrostatic precipitators (ESPs) are frequently employed to filter out airborne contaminants. ESPs are generally utilized in a variety of industrial applications to collect particles that shouldn't be released into the atmosphere. Although while the particle removal efficiency for small particles (approximately 0.2 μm) has been very low, ESPs can achieve above 99% efficiency and need relatively little energy to operate [1–6].

A number of crucial parts work together in electrostatic precipitators to clean up factory fumes. Electrodes for discharging, plates for collecting, a high-voltage power source, and a means of cleaning are all part of the system. Particles are charged by the discharge electrodes and are then attracted to and collected by the collecting plates, which have the opposite charge [7]. Ionization is achieved with the use of a high-voltage power source, and the cleaning mechanism gets rid of the particles that have accumulated on the plates [1–6]. Electrostatic precipitators (ESPs) can be categorized into two types based on the number of stages and the geometric configuration of their collection plates. ESPs can be classified as single-stage or two-stage based on the number of the stages for charging section and collecting section. On the other hand, ESPs can be classified as plate-type, tubular, and wire-type based on the geometric configuration of their collection plates. Plate-type ESPs employ flat or corrugated plates for particle collection, tubular ESPs use cylindrical tubes, and wire-type ESPs use wires to create an ionizing corona for charging the particles which are then collected on grounded plates [8]. Particle charging, particle motion, particle collecting, and particle elimination make up the five main elements of electrostatic precipitation [9–11]. The design of collecting electrodes and corona wires, as essential components of the electrostatic precipitator, has a significant impact on ESP performance. As a result, many investigations are being conducted in order to improve understanding, counteract the inadequacies of ESPs, and adjust the designs of the collecting electrodes and corona wires [1]. The arrangement of discharge electrodes, wire-to-wire spacing, and wire-to-plate spacing are all being studied. Zhiyuan Ning investigated

Cite this article as: Bani Fayyad, M., Iváncsy T. "Numerical Study of the Influence of Using Semicircular Corrugated Collecting Plate and Inverted Semicircular Corrugated on the Electrostatic Precipitator", Periodica Polytechnica Electrical Engineering and Computer Science, 68(2), pp. 124–134, 2024. https://doi.org/10.3311/PPee.22592

the influence of the arrangement on the airflow mode and the efficiency of ESP collection [12]. On high-temperature electrostatic precipitators, Xi Xu compared the impacts of three distinct structures [13]. Using experiments and numerical computations, Park and Kim investigated the flow properties of a simple geometric model ESP [14–17]. Numerous investigations (numerical and experimental) have examined the configurations of ESP's collecting plates. The performance of the electrostatic precipitator was enhanced by utilizing a large dust collector and modifying its geometry [18]. However, the flat collecting plate ground electrode shape is assumed in many investigations. Nonetheless, a few experiments have been motivated to assess electrohydrodynamic (EHD) flow in ESPs utilizing non-flat collection plates [15, 19–24]. Different shapes of collecting plates were numerically studied such as C-type, wavy, triangular, and W-type, and crenelated plates [1–6, 19, 25–27]. Electric field parameters, airflow distribution uniformity, and collection efficiency were examined for seven dust-collecting plates [17].

Understanding the electrical characteristics and particle movement in electrostatic precipitators (ESPs) has been made easier with the development of increasingly sophisticated and comprehensive numerical approaches due to advancements in numerical technology [3, 26]. Due to their adaptability, affordability, and increased dependability, numerical simulations are preferred over practical methods [3, 26]. Numerical validation techniques for electrostatic precipitators (ESPs) such as computational methods like Computational Fluid Dynamics (CFD) [28, 29]. These techniques simulate gas flow patterns, particle behavior, electric field distribution, and particle charging, and include mesh sensitivity analysis to enhance the accuracy of simulations [6, 30].

Some studies were investigated the corrugated collecting plates to improve the particle collection efficiency, for instance Zhou examined the corrugated type and it was compared to different types of collecting plates for a range of particles (1–10 μm), On the other hand, a recent study presented a new electrostatic precipitator (ESP) to capture dangerous biomass combustion submicron particles. The research found that the new ESP with semi-circular corrugated plates controls vortices and has higher collection efficiency than the flat plate ESP [31]. However, by adopting the semi-circular corrugated plates (SCPs) and their privileges and increasing the number of semi-circular corrugated parts and using 7 circular corona discharge wires, the particle collection efficiency will be improved, and comparing this model with another type of inverted Semi-circular corrugated collecting plates (InvSCPs). In this paper, three types of ESPs were simulated, and the SCP and InvSCP designs were compared to the FPs to investigate how the collecting electrode design affects electrostatic precipitator properties. The study found that using SCP resulted in the highest particle collection efficiency compared to InvSCP and FP for the same range of particles.

2 Numerical study

2.1 Corona discharge

In ESP, the electric field is non-uniform. It can be solved quantitatively using the Poisson equation and the charge-conservation equation, which are written in terms of electric potential and space-charge density [1–6]:

$$\frac{\partial \rho_q}{\partial t} + \nabla \times \boldsymbol{J} = 0, \tag{1}$$

$$\boldsymbol{J} = z_q \mu \rho_q \boldsymbol{E} + \rho \boldsymbol{u}, \tag{2}$$

$$\varepsilon_0 \nabla^2 V = -\rho_q, \tag{3}$$

$$\boldsymbol{E} = -\nabla V. \tag{4}$$

In order to solve these equations, boundary conditions must be constructed; Peek's equation Eq. (5) is used to define the first boundary condition, which specifies that the onset electric field is dependent on the radius of the corona wire and the operating environment parameters. Since $\boldsymbol{n} \times \boldsymbol{E} = E_0$, we can easily determine E_0 using Eq. (5). On the other hand, the corona wires voltage and grounded collection plate voltage establish the other boundary conditions, where $V = V_0$ for the discharge electrode and $V = 0$ for the grounded electrode.

$$E_0 = 3 \times 10^6 \delta \left(1 + 0.03 \Big/ \sqrt{\delta \times r_w}\right) \tag{5}$$

$$\delta = \frac{T_0}{T} \times \frac{P}{P_0} \tag{6}$$

2.2 Fluid flow model

Since laminar flows are hypothetically ideal, a turbulent flow was used in this research. The RNG technique and the k-epsilon turbulence model are then employed to establish an incompressible, stable, and turbulent flow as Eqs. (7)–(9) [1–6]. High Reynolds numbers (Re) characterize turbulent flows, which can be solved by applying the Reynolds-averaged Navier-Stokes (RANS) equations.

$$\rho \nabla \times \boldsymbol{u} = 0 \tag{7}$$

$$\rho \frac{\partial \boldsymbol{u}}{\partial t} + \rho\left(\boldsymbol{u} \times \nabla\right)\boldsymbol{u} = \nabla \times \left[-p\boldsymbol{I} + \mu\left(\nabla \boldsymbol{u} + \left(\nabla \boldsymbol{u}\right)^{T}\right)\right] + \boldsymbol{F}_{\mathrm{EHD}} \tag{8}$$

$$\boldsymbol{F}_{\mathrm{EHD}} = \rho_q \boldsymbol{E} \tag{9}$$

2.3 Particle charging and movement

Another essential topic is particle charging, which occurs when particles cross and enter the ionized field and may be explained by numerous mathematical equations. These models were used to estimate particle charges and charging rates. Particle charging methods operate in two ways. These particles can be charged by diffusion or field charging. Thermal movement and ion collisions charge dust particles [32, 33]. In this research, the Lawless model, which considers large and tiny particles, is used to predict particle charging process [1–3, 5, 6, 34].

$$\tau_c \frac{dZ}{dt} = \begin{cases} \dfrac{v_s}{4\varepsilon_0}\left(1 - \dfrac{v_e}{v_s}\right)^2 + f_a, & \left(|v_e| \le |v_s|\right) \\ \dfrac{v_e - v_s}{\exp\left(v_e - v_s\right) - 1} f_a, & \left(|v_e| > |v_s|\right) \end{cases} \tag{10}$$

$$\tau_c = \frac{e^2}{4\pi\rho_q \mu k_B T_i} \tag{11}$$

$$v_s = 3w_e \frac{\varepsilon_{r,p}}{\varepsilon_{r,p+2}} \tag{12}$$

$$v_e = \frac{Ze^2}{4\pi\varepsilon_0 r_p k_B T_i} \tag{13}$$

$$w_e = \frac{e r_p |E|}{k_B T_i} \tag{14}$$

$$f_a\left(w_e\right) \equiv \begin{cases} \dfrac{1}{\left(w_e + 0.475\right)^{0.575}}, & w_e \ge 0.525 \\ 1, & w_e < 0.525 \end{cases} \tag{15}$$

According to the particle movement, each charged particle will be affected primarily by electric force and mechanical force arising from fluid movement; in addition, gravity is ignored as particles move through the ESP. In Eq. (18) and Eq. (20), we find the definitions of these two classes of forces . Because of the attractive forces between charges of different poles, charged particles will rush to the collecting plates when electrical forces are present [1–6]. Until they were charged, the particles would naturally go in the direction of the gas flow. Particle motion can be described by Newton's second law, which can be written as Eq. (16).

$$\frac{d\boldsymbol{x}}{dt} = \boldsymbol{v} \tag{16}$$

$$\frac{d}{dt}\left(m_p \boldsymbol{v}\right) = \boldsymbol{F}_t \tag{17}$$

The drag force $\boldsymbol{F}_D$(N) is specified by Eq. (18), which incorporates corrections defined by the Cunningham-Millikan-Davis model [17], whereas the electric force $\boldsymbol{F}_e$(N) is given by Eq. (20).

$$\boldsymbol{F}_D = \frac{1}{\tau_p S} m_p \left(\boldsymbol{u} - \boldsymbol{v}\right) \tag{18}$$

$$\tau_p = \frac{4\rho_p d_p^2}{3\mu C_D \,\mathrm{Re}_r} \tag{19}$$

$$\boldsymbol{F}_e = eZ\boldsymbol{E} \tag{20}$$

2.4 Particle collection

In actuality, the performance of the ESP is determined by the ratio of captured to uncaptured particles. This can be evaluated via probability theory. For example, Eq. (21) can be used to compute particle collection efficiency for a duct-type ESP [32, 35]. However, in this study the particle collection efficency was detected by using the counter detector at the outlet of this model in the COMSOL software [1–6].

$$\eta = 1 - \exp\left(-\frac{L \times |\boldsymbol{v}|}{s \times |\boldsymbol{u}|}\right) \tag{21}$$

2.5 Geometrical arrangements and parameters definition

In this study, the finite element approach was utilized to simulate a model of electrostatic precipitators in 2D geometries using the COMSOL Multiphysics software (FEM). Table 1 displays the measured values for the study's variables. Where, 2 cases of corrugated collecting plates were modeled and compared with the flat plate collecting type as shown in Fig. 1. The simulation was categorized into three phases: a static electrostatics simulation, a static airflow simulation, and a time-dependent particle motion simulation utilizing a particle tracing module.

Table 1 Specific geometry for the ESP arrangement

Description	Value
Length (mm)	750
Distance between the collecting plates (mm)	150
Distance between two corona wires (mm)	75
Number of corona electrodes	7
Corona electrode radius (mm)	0.75
Applied voltage (kV)	45
Air turbulent fluid flow, avg velocity (m/s)	1
Temperature (K)	293.15
Gas density (kg m^{-3})	1.2
Gas viscosity (Pa s)	1.85×10^{-5}
Pressure (atm)	1
Particle radii (μm)	0.01^{-5}
Particle density (kg m^{-3})	2100
Particle relative permittivity	5
Reduced ionic mobility (m^{-1} V^{-1} s^{-1})	3×10^{21}
Space charge density, initial value (C m^{-3})	1×10^{-5}

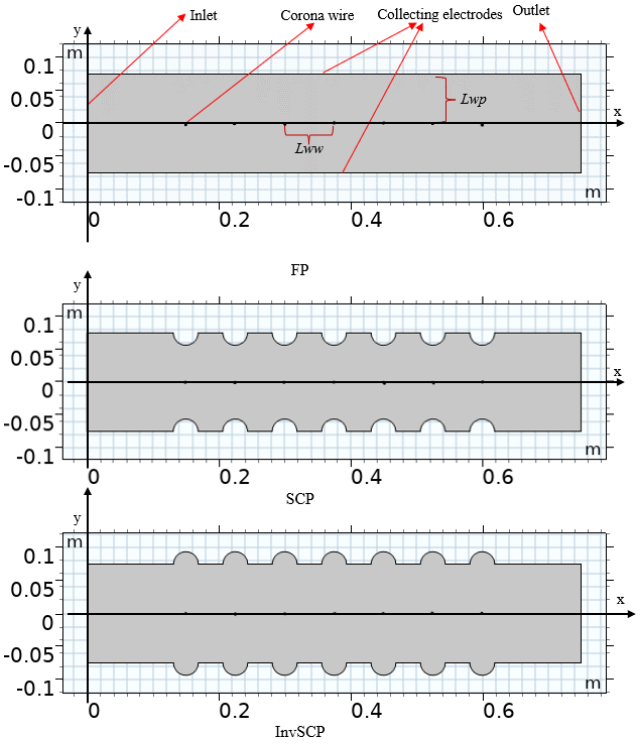

Fig. 1 Geometrical arrangements of FP, SCP, and InvSCP

2.6 Mesh settings

This study compares the effects of using Semicircular Corrugated Plates (SCPs) and inverted Semicircular Corrugated Plates (InvSCPs), against Flat Plates (FPs) as a reference case, based on where they are located in relation to the corona wires. The idea is to analyze how various collecting electrode designs influence an electrostatic precipitator's efficiency.

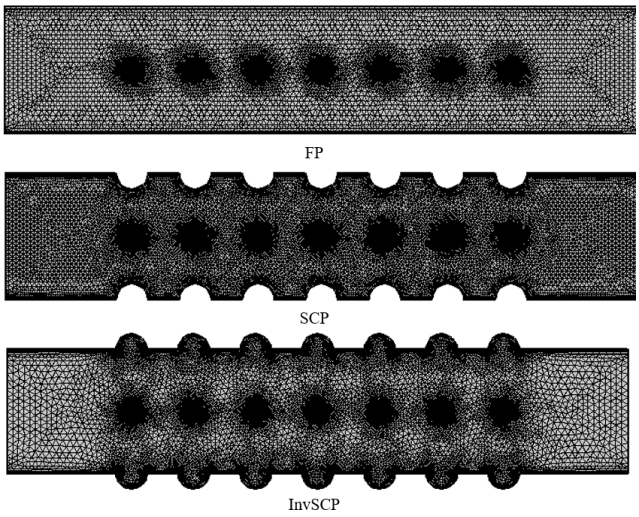

Fig. 2 Mesh construction of FP, SCP, and InvSCP

Since corona electrodes are rather large, a greater number of elements are specified in their immediate vicinity. The gradient calculations in that region benefit greatly from the denser mesh that was constructed for that purpose. For the SCP the total number of triangular elements is 29542 for a mesh area of 0.1048 m^2 and 2460 quads and the mesh size is 31948. In addition, in the InvSCPs, there are a total of 28712 triangular elements, 2436 quads, and the size of mesh is 31148, covering mesh areas of 0.1202 m^2. While the total mesh size for FP is 24269, the number of triangular elements is 22296, and the number of quads is 1810. Fig. 2 shows the mesh construction for SCP, InvSCP, and FP. To ensure the simulation, the mesh independent was performed for the SCP, InvSCP, and FP coarse, normal, and fine, where the results for all meshes were identical.

3 Results and discussion

3.1 Validation with Penney and Kihm

To ensure the accuracy of our findings, we compared the results of Penney's research experiments with the distribution of electric potential derived from a numerical model [36]. The simulation was defined by the following geometric parameters: 0.15 mm corona wire radius, 150 mm distance between corona wires, 228.6 mm width, and 609.6 mm length. Experiment results for 25.5–34.5 kV are in agreement with the numerical solution as shown in Fig. 3.

Moreover, experimental data from Kihm are used to verify the accuracy of the current model as seen in Fig. 4. Kihm's

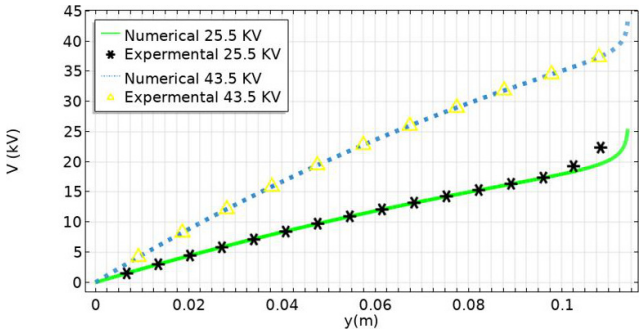

Fig. 3 Validation of the electrical potential with experimental data

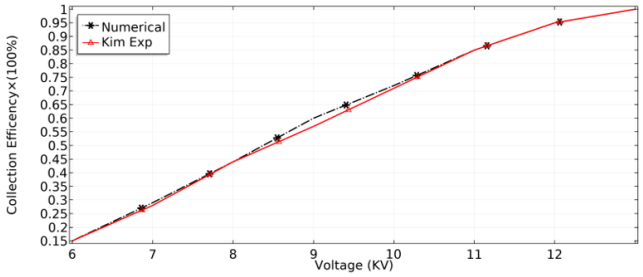

Fig. 4 Validation of the ESP efficiency (kV) with experimental data

setup included eight corona discharge wires. The operational voltages are between 6 kV and 13 kV. Plates are 400 mm in length and 50 mm in height, while the diameter of each corona wire is 0.05 mm, the space between the wire and the plate is 25 mm, the space between wires is 50 mm [37].

On the other side, by improving the SCPs that were modeled using 3 semi-circular corrugated parts with 4 corona wires [31] to a new design using 4 semi-circular corrugated parts with 4 corona wires, the new design will enhance the particle collection efficiency at the same voltage level as shown in Fig. 5. The reference [31] used 4 corona wires arrangements with 3 semicircular corrugated parts; where the 1st and 4th corona wires are under the semi corrugated part, while the 2nd and the 3rd corona wires are not below the corrugated parts. While, if 4 SCP parts with 4 corona wires are used, the particle collection efficiency will be improved as shown in Fig. 5. It is very important to notice that the location of the corona wires under these semi corrugated parts which increases the collection efficiency. As result, using 7 corona wires with 7 SCP parts will be a superior if it will be compared at the same voltage level to [31].

3.2 Fluid flow

The fluid flow in the ESP has the great influence in the particle collection efficiency of the ESP. Fig. 6 shows the fluid flow of 3 types of collecting plates, where the average air flow was 1 m/s, it can be noticed that the highest

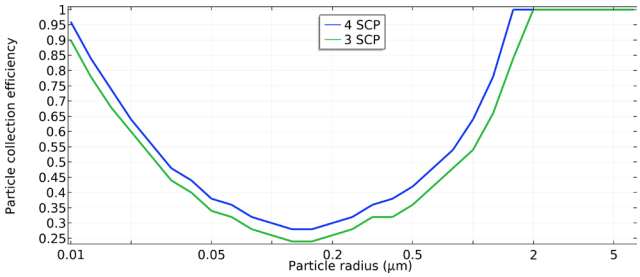

Fig. 5 Particle collection efficiency – particle radius for 4 SCP parts and 3 SCP parts when using 30 kV

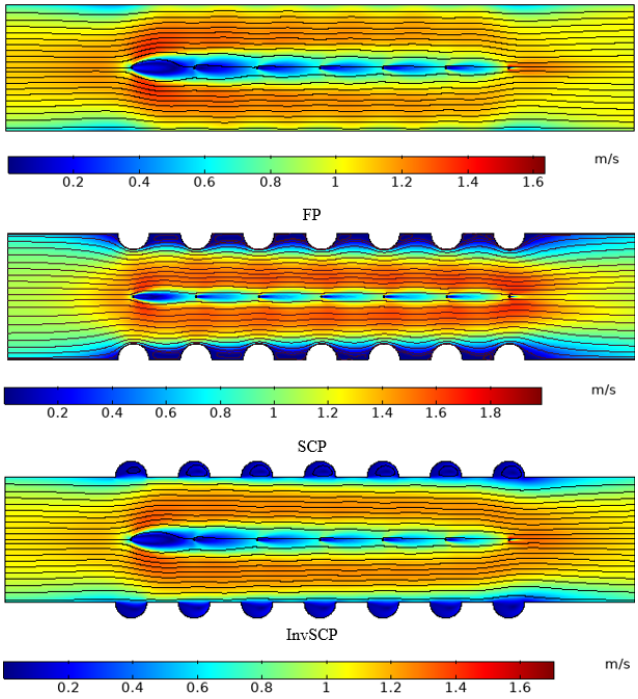

Fig. 6 Fluid flow of the FP, SCP, and InvSCP

air flow is when using SCP, because the shape of the semi corrugated parts, which produces a narrow path for the air flow compared to FP and InvSCP.

3.3 Electrical Potential and electrical field

Simulation measurements were performed within the ESP at 45 kV applied voltage for corona wires and 0 V for collecting electrodes to investigate the electric potential and electric field at the same range of voltage. The distribution of the electric potential for SCP, InvSCP, and FP reference is shown in Fig. 7. Where the highest value around the corona wires, and the values decrease toward the collecting electrode. Figs. 8 to 10 illustrate the electrical potential distributions for each individual case by using 3 y cutlines: y = 0.01, y = 0.03, y = 0.045 m. It is clear that the distributions of electrical potential for FP and InvSCP are very close to each other, while, for the same

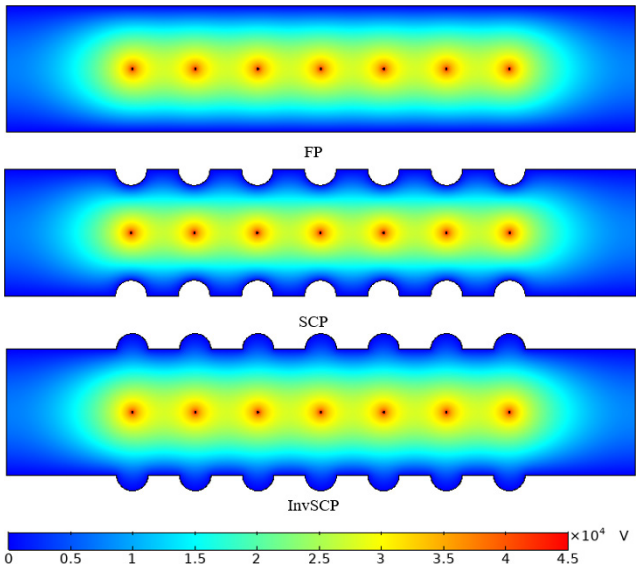

Fig. 7 Electrical potential of the FP, SCP, and InvSCP

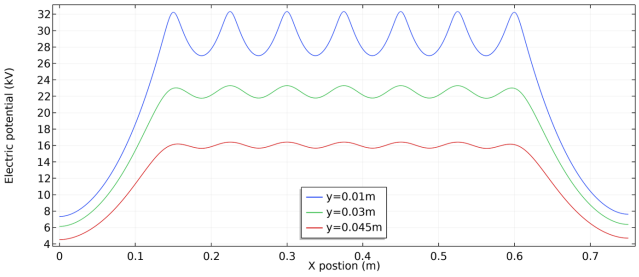

Fig. 8 Electrical potential distributions of the FP

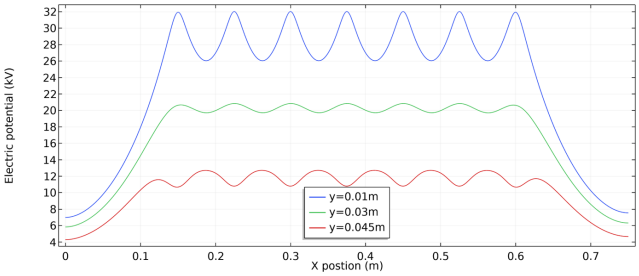

Fig. 9 Electrical potential distributions of the SCP

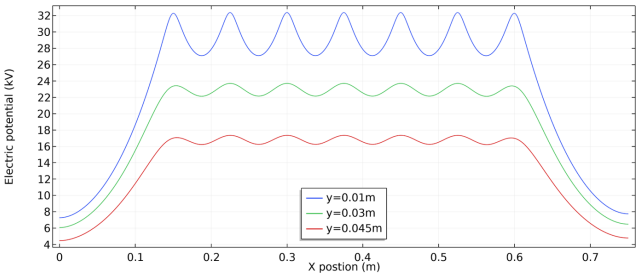

Fig. 10 Electrical potential distributions of the InvSCP

cutline $y = 0.045$ m, SCP's electrical potential distribution is the smallest value. However, Fig. 11 shows the electrical distributions of $y = 0.045$ m for all the cases together. The lowest distribution values are located at the midpoint between the corona wires, while the highest values on the locations of corona wires. For the electrical field distributions, Fig. 12 shows the distributions for 3 types when using x-cutline; $x = 0.6$ m, the x-cutline starts from the position of 7th corona wire to 0.045 m. It is noticed that the highest values is SCP.

3.4 Space charge density and current density

Fig. 13 depicts the distributions of the space charge density for 3 types of collecting plates, where the charge density drastically dropped as moving closer to the plates. In addition, it is obvious that the SCP values are greater than FP and InvSCP cases. If it is taken a vertical cutline; $x = 0.6$ m, Fig. 14 shows the distribution of the SCP, InvSCP, and FP. Where the space charge density around the 7th corona wire position is 32×10^{-5} C/m^3, on the other hand, at the same position, the values for FP and InvSCP are 18×10^{-5} C/m^3 and 16×10^{-5} C/m^3, respectively. On the other hands, comparing the current–voltage (I–V) curves for each case allows for evaluating the ESP's performance. Fig. 15 shows the I–V curve for 3 types. The figure shows that increasing the wire-to-plate distance at a voltage level substantially raises the current density. The highest curve was SCP, while the lowest was InvSCP. Fig. 16 shows the current density for 3 types by using a horizontal cutline $y = 0.045$ m.

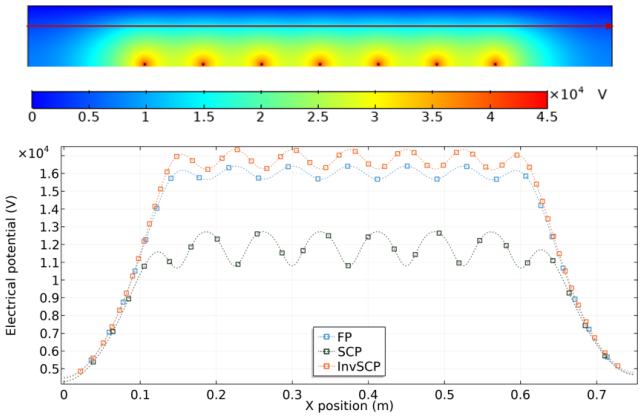

Fig. 11 Electrical potential distributions of the FP, SCP, InvSCP

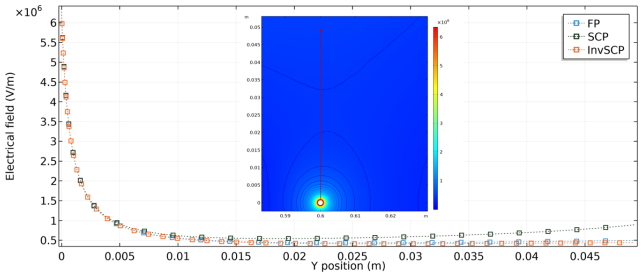

Fig. 12 Electrical field with Y position of the FP, SCP, InvSCP

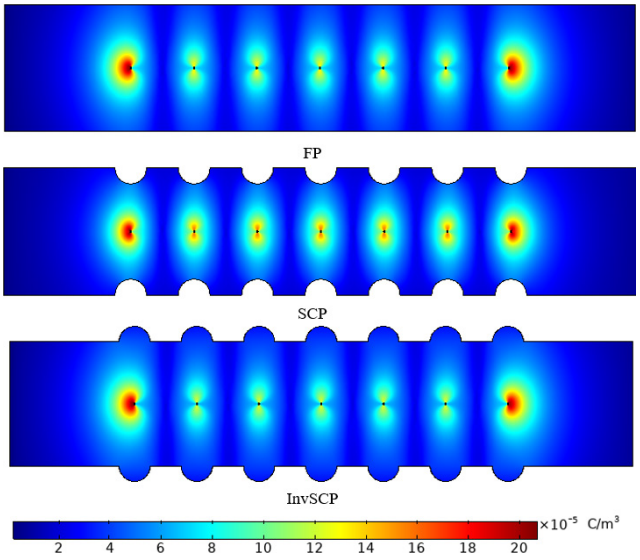

Fig. 13 Space charge density of the FP, SCP, InvSCP

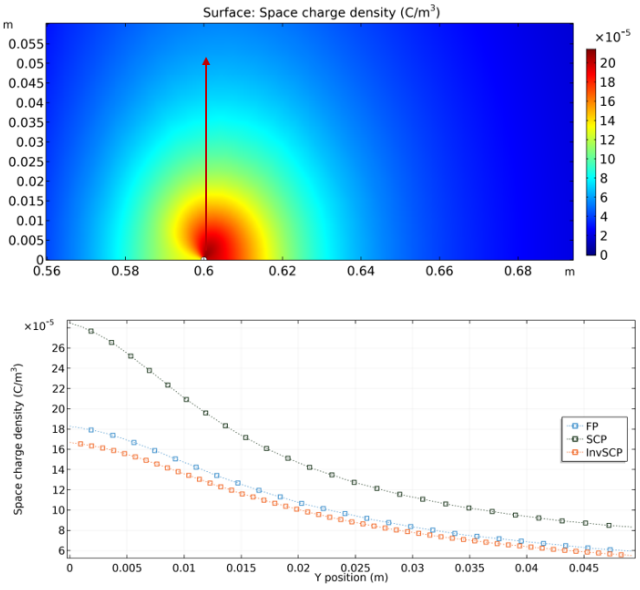

Fig. 14 Space charge density of the FP, SCP, InvSCP

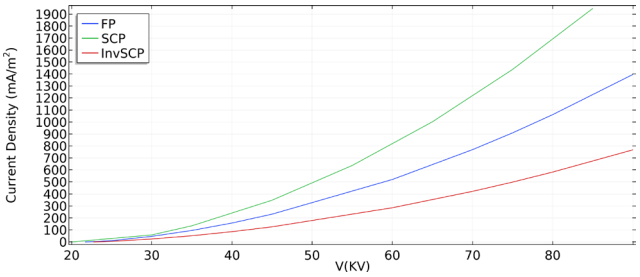

Fig. 15 Current density vs electrical potential for FP, SCP, InvSCP

3.5 Particle trajectories

The electric field, space charge density, and flow properties affect particle behavior. Semi-corrugated and inverted semi-corrugated grounding electrodes' effects on particle

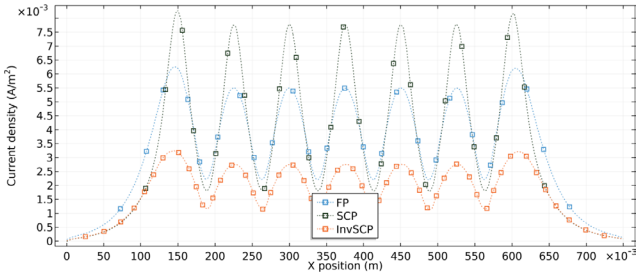

Fig. 16 Current density of the FP, SCP, InvSCP

trajectories are also examined. When particles reach the first corona wire, their paths shift. Particles enter the ESP through the inlet, move parallel to the grounding plates, and alter again. The second corona electrode traps more particles. Fig. 17 shows particle trajectories in ESPs for 3 collecting electrode types for 0.2 μm and 2 μm at 45 kV.

3.6 Accumulated charge number and particle collection efficiency

As can be seen in Fig. 18, there is a direct relationship between particle size and the total amount of particles accumulated. The best example is SCP, because it is evident that a SCP shape will result in a greater accumulation of particles as compared to FP and InvSCP at 45 kV. If it is taken the same size of the particles as 4 μm, the accumulated charge number are 13000, 11000, and 10500 for SCP, FP, and InvSCP, respectively.

Fig. 19 displays the SCP and InvSCP model results for particle collecting efficiency. To get a specific U-form of particle collecting efficiency versus particle radius, the FPs findings were utilized as a benchmark, and the particle range was set at 0.01–0.5 μm. In this study the particle collection efficency was detected by using the counter detector at the outlet of this model in the COMSOL software. It can be noticed that using SCP has the highest particle collection efficency compared to FP and InvSCP when they are compared at 45 kV. In addition, the lowest range of particles is 0.1–0.15 μm for SCP with 68%, while this range is wider for FP , 0.1–0.2 μm with 64%, however, for InvSCP the range is 0.1–0.2 μm with 56%. According to the size of the particle which the ESP efficency begins to reach 100%, for SCP the size of particle is 0.5 μm, while they are 0.63 μm and 0.79 μm for FP and InvSCP, respectively.

4 Conclusion

In this paper, three types of ESPs were simulated, and the SCPs and InvSCP designs were compared to the FPs to investigate how the collecting electrode design affects electrostatic precipitator properties. The study found that

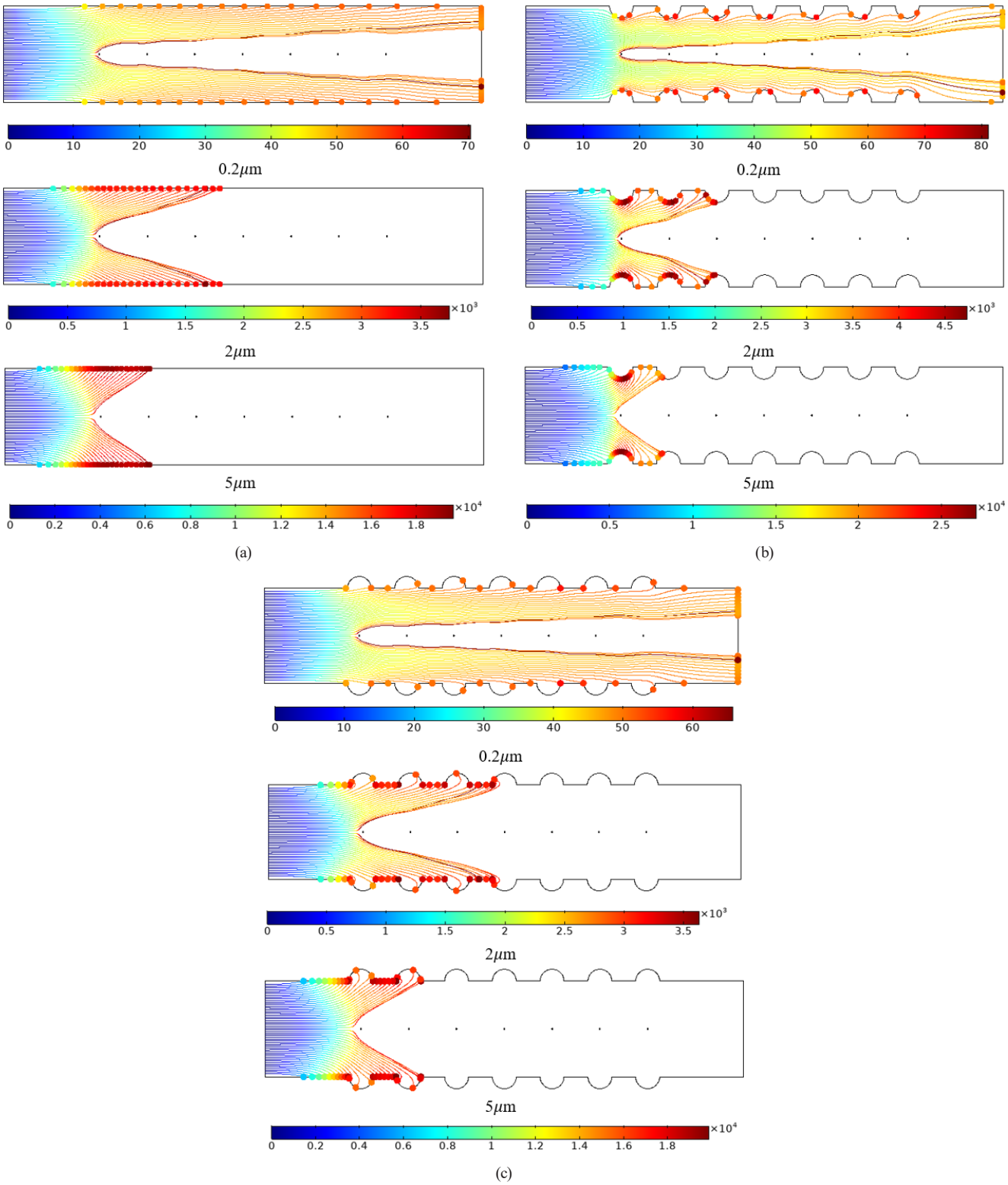

Fig. 17 Particle trajectories of the (a) FP, (b) SCP, and (c) InvSCP for radii 0.2, 2, 5 μm

using the same number of SCP parts with the number of corona wires resulted in the highest particle collection efficiency compared to InvSCP and FP for the same range of particles. Also, it is very important to notice that the location of the corona wires under these semi-corrugated parts which increases the collection efficiency. In addition, a SCP model results in a greater accumulation of particles as compared to FP and InvSCP. In this study the particle

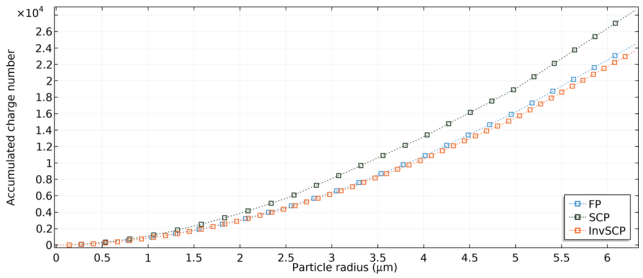

Fig. 18 Accumulated charge number of the FP, SCP, and InvSCP

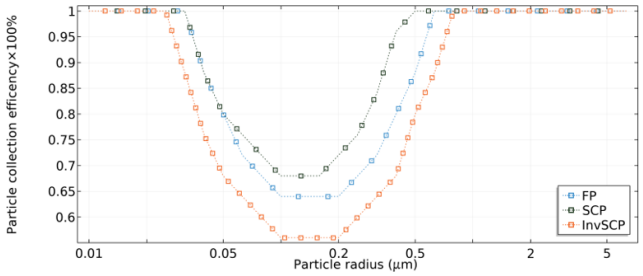

Fig. 19 Particle collection efficiency of the FP, SCP, and InvSCP

collection efficency was detected by using the counter detector at the outlet of this model in the COMSOL software. It can be noticed that using SCP has the highest particle collection efficency compared to FP and InvSCP. According to the size of the particle which the ESP efficency begins to reach 100%, for SCP the size of particle is 0.5 μm, while they are 0.63 μm and 0.79 μm for FP and InvSCP, respectively.

However, this study will lead to investigate further studies of corrugated types, to get the best design of ESP collecting electrodes.

Acknowledgement

The project presented in this article is supported by Stipendium Hungaricum.

Nomenclature

ρ_q	Space charge density (C/m^3)
$\boldsymbol{z_q}$	Charge number
μ	Ion mobility (m^2/V s)
$\boldsymbol{E}$	Electric field intensity (V/m)
$\boldsymbol{u}$	Fluid velocity (m/s)
E_0	Onset electric field (V/m)
V	Electric potential (V)
$\boldsymbol{n}$	Normal unit vector
$\boldsymbol{J}$	Current density (A/m^2)
V_0	Applied electric potential (V)
ε_0	Free-space permittivity (F/m)
δ	Gas relative density
r_w	Corona wire radius (m)
T_0	Standard temperature (K)
T	Operating temperature (K)
P	Operating pressure (mmHg)
P_0	Standard pressure (mmHg)
ρ	Fluid density (Kg/m^3)
p	Pressure (Pa)
$\boldsymbol{F}_{\text{EHD}}$	Electrohydrodynamic force (N)
I	Identity matrix
μ_f	Dynamic viscosity (Kg/m s)
τ_c	Charging time (s)
Z	Accumulated charge number
v_s	Dimensionless particle charges
v_e	Self-potential of the particle
f_a	Analytic fitting function
e	Elementary charge
k_B	Boltzmann's constant
T_i	Ion temperature (eV)
w_e	Dimensionless electric field intensity
$\varepsilon_{r,p}$	Particle relative permittivity
$\boldsymbol{x}$	Particle position (m)
$\boldsymbol{v}$	Particle velocity (m/s)
m_p	Particle mass (kg)
$\boldsymbol{F}_t$	Total particle force (N)
$\boldsymbol{F}_D$	Drag force (N)
τ_p	Particle velocity–time response (s)
S	Drag correction coefficient
d_p	Particle diameter (m)
C_D	Cunningham correction factor
R_{er}	Reynolds number
F_e	Electric force (N)
η	Particle collection efficiency
L	Collecting plate length (m)
L_{ww}	Wire–wire space (m)
L_{wp}	Wire–plate space (m)

References

[1] Bani Fayyad, M. M., Asipuela González, A. G., Iváncsy, T. "Numerical study of wavy collecting electrodes with different shapes of corona electrodes", In: 2022 IEEE 5th International Conference and Workshop Óbuda on Electrical and Power Engineering (CANDO-EPE), Budapest, Hungary, 2022, pp. 37–42. ISBN 979-8-3503-4619-0
https://doi.org/10.1109/CANDO-EPE57516.2022.10046364

[2] Fayyad, M. B., González, A. A., Iváncsy, T. "The effects of the corona wire distribution with triangular collecting plates on the characteristics of electrostatic precipitators", In: 2022 International Conference on Diagnostics in Electrical Engineering (Diagnostika), Pilsen, Czech Republic, 2022, pp. 1–7. ISBN 978-1-6654-8082-6
https://doi.org/10.1109/Diagnostika55131.2022.9905103

[3] Fayyad, M. B., González, A. A., Iváncsy, T. "Numerical study of a duct-type ESP with W-type collecting electrodes and different circular corona electrodes radius", In: 2022 8th International Youth Conference on Energy (IYCE), Eger, Hungary, 2022, pp. 1–5. ISBN 978-1-6654-8721-4
https://doi.org/10.1109/IYCE54153.2022.9857530

[4] Asipuela, A., Bani Fayyad, M., Iváncsy, T. "The Effect of Corona Wire Position and Radius in a Duct-Type ESP with Wavy Collecting Plates", International Journal of Electrical and Electronic Engineering & Telecommunications, 11(4), pp. 262–268, 2022.
https://doi.org/10.18178/ijeetc.11.4.262-268

[5] Asipuela, A., Fayyad, M. B., Iváncsy, T. "Study and Numerical Simulation of a Duct-type ESP with Wavy Collecting Electrodes and Different Circular Corona Electrodes Radius", In: 2022 IEEE 4th International Conference on Dielectrics (ICD), Palermo, Italy, 2022, pp. 234–238. ISBN: 978-1-6654-1833-1
https://doi.org/10.1109/ICD53806.2022.9863610

[6] Fayyad, M. B., González, A. A., Iváncsy, T. "Numerical study of the influence of using crenelated collecting plates on the electrostatic precipitators", Journal of Electrostatics, 123, 103811, 2023.
https://doi.org/10.1016/j.elstat.2023.103811

[7] Mizuno, A. "Electrostatic precipitation", IEEE Transactions on Dielectrics and Electrical Insulation, 7(5), pp. 615–624, 2000.
https://doi.org/10.1109/94.879357

[8] Badran, M., Mansour, A. M. "Evaluating Performance Indices of Electrostatic Precipitators", Energies, 15(18), 6647, 2022.
https://doi.org/10.3390/en15186647

[9] Lee, G.-H., Hwang, S.-Y., Cheon, T.-W., Kim, H.-J., Han, B., Yook, S.-J. "Optimization of pipe-and-spike discharge electrode shape for improving electrostatic precipitator collection efficiency", Powder Technology, 379, pp. 241–250, 2021.
https://doi.org/10.1016/j.powtec.2020.10.044

[10] Tachibana, N., Matsumoto, Y. "Intermittent energization on electrostatic precipitators", Journal of Electrostatics, 25(1), pp. 55–73, 1990.
https://doi.org/10.1016/0304-3886(90)90037-V

[11] Podliński, J., Niewulis, A., Mizeraczyk, J. "Electrohydrodynamic flow and particle collection efficiency of a spike-plate type electrostatic precipitator", Journal of Electrostatics, 67(2–3), pp. 99–104, 2009.
https://doi.org/10.1016/j.elstat.2009.02.009

[12] Ning, Z., Podlinski, J., Shen, X., Li, S., Wang, S., Han, P., Yan, K. "Electrode geometry optimization in wire-plate electrostatic precipitator and its impact on collection efficiency", Journal of Electrostatics, 80, pp. 76–84, 2016.
https://doi.org/10.1016/j.elstat.2016.02.001

[13] Xu, X., Zheng, C., Yan, P., Zhu, W., Wang, Y., Gao, X., Luo, Z., Ni, M., Cen, K. "Effect of electrode configuration on particle collection in a high-temperature electrostatic precipitator", Separation and Purification Technology, 166, pp. 157–163, 2016.
https://doi.org/10.1016/j.seppur.2016.04.039

[14] Park, S. J., Kim, S. S. "Electrohydrodynamic Flow and Particle Transport Mechanism in Electrostatic Precipitators with Cavity Walls", Aerosol Science and Technology, 33(3), pp. 205–221, 2000.
https://doi.org/10.1080/027868200416204

[15] Park, S. J., Kim, S. S. "Effects of Electrohydrodynamic Flow and Turbulent Diffusion on Collection Efficiency of an Electrostatic Precipitator with Cavity Walls", Aerosol Science and Technology, 37(7), pp. 574–586, 2003.
https://doi.org/10.1080/02786820300928

[16] Zhu, Y., Gao, M., Chen, M., Shi, J., Shangguan, W. "Numerical simulation of capture process of fine particles in electrostatic precipitators under consideration of electrohydrodynamics flow", Powder Technology, 354, pp. 653–675, 2019.
https://doi.org/10.1016/j.powtec.2019.06.038

[17] Chen, B., Guo, Y., Li, H., Liu, B., He, Y., Zhao, H. "Insights into the effect of the shape of collecting plates on particle precipitation processes in an electrostatic precipitator", Journal of the Air & Waste Management Association, 70(9), pp. 892–903, 2020.
https://doi.org/10.1080/10962247.2020.1768965

[18] Ko, J.-H., Ihm, S.-K. "A Two-Dimensional Model for Polydisperse Particles on the Effective Migration Rate of the Electrostatic Precipitator with Wider Plate-Spacing", Aerosol Science and Technology, 26(5), pp. 398–402, 1997.
https://doi.org/10.1080/02786829708965440

[19] Lami, E., Mattachini, F., Gallimberti, I., Turrib, R., Tromboni, U. "A numerical procedure for computing the voltage-current characteristics in electrostatic precipitator configurations", Journal of Electrostatics, 34(4), pp. 385–399, 1995.
https://doi.org/10.1016/0304-3886(94)00030-Z

[20] Bernstein, S., Ushimaru, K., Geller, E. W. "Advanced electrode design for electrostatic precipitators", Flow Research Co., South Kent, WA, USA, Rep. DOE/EV/10506-T1, 1980.
https://doi.org/10.2172/6867624

[21] Fujishima, H., Ueda, Y., Tomimatsu, K., Yamamoto, T. "Electrohydrodynamics of spiked electrode electrostatic precipitators", Journal of Electrostatics, 62(4), pp. 291–308, 2004.
https://doi.org/10.1016/j.elstat.2004.05.006

[22] Wen, T. Y., Krichtafovitch, I., Mamishev, A. V. "Numerical study of electrostatic precipitators with novel particle-trapping mechanism", Journal of Aerosol Science, 95, pp. 95–103, 2016.
https://doi.org/10.1016/j.jaerosci.2016.02.001

[23] Liu, L., Gu, X., Zhang, L., Sun, T., Cao, Z., Yu, B., Li, J., Zhang, L., Xu, W., Bu, S., Zhang, L. "Experiment and numerical simulation investigation on wire-plate electrostatic precipitator with expanded-shrunk spoilers", Powder Technology, 395, pp. 60–70, 2022. https://doi.org/10.1016/j.powtec.2021.09.064

[24] Shen, H., Yu, W., Jia, H., Kang, Y. "Electrohydrodynamic flows in electrostatic precipitator of five shaped collecting electrodes", Journal of Electrostatics, 95, pp. 61–70, 2018. https://doi.org/10.1016/j.elstat.2018.08.002

[25] Fayyad, M. B., Asipuela, A., Iváncsy, T. "The effect of the corona wire distribution with W-type of collecting plates on the characteristics of electrostatic precipitators", Journal of Electrostatics, 125, 103841, 2023. https://doi.org/10.1016/j.elstat.2023.103841

[26] Choi, H. Y., Park, Y. G., Ha, M. Y. "Numerical simulation of the wavy collecting plate effects on the performance of an electrostatic precipitator", Powder Technology, 382, pp. 232–243, 2021. https://doi.org/10.1016/j.powtec.2020.12.070

[27] Zhou, W., Jiang, R., Sun, Y., Chen, B., Liu, B. "Study on multi-physical field characteristics of electrostatic precipitator with different collecting electrodes", Powder Technology, 381, pp. 412–420, 2021. https://doi.org/10.1016/j.powtec.2020.12.028

[28] Arif, S., Branken, D. J., Everson, R. C., Neomagus, H. W. J. P., Le Grange, L. A., Arif, A. "CFD modeling of particle charging and collection in electrostatic precipitators", Journal of Electrostatics, 84, pp. 10–22, 2016. https://doi.org/10.1016/j.elstat.2016.08.008

[29] Kılıç, M., Mutlu, M., Altun, A. F. "Numerical Simulation and Analytical Evaluation of the Collection Efficiency of the Particles in a Gas by the Wire-Plate Electrostatic Precipitators", Applied Sciences, 12(13), 6401, 2022. https://doi.org/10.3390/app12136401

[30] Asipuela González, A., Fayyad, M. B., Iváncsy, T. "The effect of combining wavy and W-type collecting electrodes on the properties of electrostatic precipitators", Journal of Electrostatics, 123, 103818, 2023. https://doi.org/10.1016/j.elstat.2023.103818

[31] Varshney, A., Mishra, N. K., Das, R. "Enhancement of collection efficiency for capturing submicron particles emitted from biomass burning: a novel design of semi-circular corrugated plate electrostatic precipitator", Biomass Conversion and Biorefinery, 13(18), pp. 17059–17074, 2023. https://doi.org/10.1007/s13399-022-02358-8

[32] White, H. J. "Industrial electrostatic precipitation", Addison-Wesley Publishing Company, Boston, MA, USA, 1963.

[33] White, H. J. "Particle charging in electrostatic precipitation", Transactions of the American Institute of Electrical Engineers, 70(2), pp. 1186–1191, 1951. https://doi.org/10.1109/T-AIEE.1951.5060545

[34] Asipuela, A., Iváncsy, T. "Study and Numerical Simulation of the Electrical Properties of a Duct-Type Electrostatic Precipitator Using Seven Circular Corona Wires: A Review", Periodica Polytechnica Electrical Engineering and Computer Science, 66(3), pp. 286–293, 2022. https://doi.org/10.3311/PPee.19482

[35] Li, S., Huang, Y., Zheng, Q., Deng, G., Yan, K. "A numerical model for predicting particle collection efficiency of electrostatic precipitators", Powder Technology, 347, pp. 170–178, 2019. https://doi.org/10.1016/j.powtec.2019.02.040

[36] Penney, G. W., Matick, R. E. "Potentials in D-C corona fields", Transactions of the American Institute of Electrical Engineers, Part I: Communication and Electronics, 79(2), pp. 91–99, 1960. https://doi.org/10.1109/TCE.1960.6368550

[37] He, Z., Dass, E. T. M. "Correlation of design parameters with performance for electrostatic Precipitator. Part I. 3D model development and validation", Applied Mathematical Modelling, 57, pp. 633–655, 2018. https://doi.org/10.1016/j.apm.2017.05.042